Open Ceramics 20 (2024) 100705

Contents lists available at ScienceDirect

Open Ceramics

journal homepage: www.sciencedirect.com/journal/open-ceramics

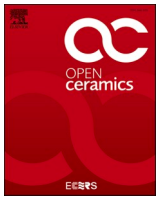

Development of aluminum oxide slurries for additive manufacturing by Bayesian optimization

Johannes Schubert [a], Pascal Friederich [b], Benedikt Burchard [a], Frederik Zanger [a,*]

[a] Karlsruhe Institute of Technology (KIT), wbk Institute of Production Science, Kaiserstraße 12, 76131 Karlsruhe, Germany
[b] Karlsruhe Institute of Technology (KIT), ITI Institute of Theoretical Informatics, AIMat group, Engler-Bunte-Ring 8, 76131 Karlsruhe, Germany

ARTICLE INFO

Keywords:
Additive manufacturing
Vat photopolymerization
Artificial Intelligence
Bayesian optimization
Slurry development

ABSTRACT

Additive manufacturing by vat photopolymerization (VPP) enables the flexible production of ceramic components. The process requires ceramic slurries consisting of a photosensitive binder system and ceramic powder. To prevent defects during debinding and sintering, the highest possible content of ceramic particles is desired. At the same time, a certain viscosity must not be exceeded to ensure the processability in the VPP process. This conflict of objectives requires a precise adjustment of the large amount of slurry constituents. Hence, an experimental slurry development and optimization is very expensive and time-consuming. Therefore, Bayesian optimization, an artificial intelligence (AI) approach, was used to enhance an experimental optimization of the slurry composition. Using this approach, it was possible to achieve in less than 40 optimization steps an aluminum oxide (Al_2O_3) slurry suitable for VPP with a content of 65 vol.% ceramic powder, the highest currently known fraction for Al_2O_3 in VPP slurries.

1. Introduction

1.1. Vat photopolymerization of ceramics

Compared to conventional manufacturing methods, the production of ceramics by additive manufacturing (AM) provides several benefits, such as the possibility to produce complex, individualized components [1]. Among ceramic AM techniques, vat photopolymerization (VPP) is a promising manufacturing method due to its ability to print dimensional accurate parts with micro-scale resolution and high surface quality [2–5]. Furthermore, VPP is capable of producing ceramics with a high relative density of more than 99% [6,7]. The starting material of the process is a ceramic slurry composed of ceramic powder and an organic binder system. Commonly used ceramic powders include aluminum oxide and zirconium oxide [8]. In the VPP process, components are manufactured layer by layer by selectively curing a ceramic slurry using ultra violet or visible light. Exposure can be point-based using a laser and scanner optics or area-based using a projector. Furthermore, a distinction is made between two basic process principles. In the first variant, the so-called bottom-up principle, the build platform is lowered step by step into the layer of liquid slurry and exposure takes place from above. In addition, a scraper ensures a uniform application of the slurry. In the second variant, the so-called top-down principle, exposure takes place from below and the build platform gradually moves upwards. For this, a glass plate is used as bottom of the vat in which the slurry is located. This process variant has the advantage that a smaller amount of resin is required and thinner layers can be realized [4].

1.2. Ceramic slurries for vat photopolymerization

The binder system is responsible for the curing of the slurry and consists of several constituents. Basically, a distinction in curing behavior can be made between radical and cationic photopolymerization, the former being applied for (meth)acrylates frequently used in ceramic slurries [9]. By exposure with light of the appropriate wavelength, a photoinitiator (PI) within the slurry is radicalized. The resulting radical binds to the functional group of a monomer and breaks it, leading to the formation of further radicals. This leads to a chain growth and can be terminated, for example, by two radicals cancelling each other out. Monomers with several functional groups are required for the crosslinking of the polymer chains formed this way. Therefore, the use of monomers with a different number of functional groups is crucial for the curing behavior of the binder [10]. In addition to the photoinitiator, a co-photoinitiator (co-PI) can support the initialization

* Corresponding author.
E-mail address: frederik.zanger@kit.edu (F. Zanger).

https://doi.org/10.1016/j.oceram.2024.100705
Received 21 October 2024; Received in revised form 12 November 2024; Accepted 12 November 2024
Available online 19 November 2024

process [11]. Furthermore, other additives can be used, such as diluents, dispersants, dyes or inhibitors, to further improve the properties of the slurry [12].

The composition of the ceramic slurry has a major influence on its processability in the VPP process and the final component properties. After completion of the VPP process, the component is initially available as a green part and must undergo further post-processing steps. During debinding, the organic content is removed from the green part, while the final component properties are achieved during sintering.

Since debinding and sintering lead to volume shrinkage, a high solid content is aimed for in the ceramic slurry in order to maintain a high component accuracy. In addition, a high solid content reduces the risk of cracks during debinding and the relative density of the sintered component is maximized [13,14]. Besides the high solid content, the ceramic slurry must not exceed a certain viscosity in order to be workable in VPP. A too high viscosity would impede the recoatability, i.e. the application of thin slurry layers for building up the component [15]. However, increasing the solid content generally lead to higher viscosities, why a compromise must be found [16]. In order to reduce the viscosity of a ceramic slurry while maintaining a high solid content, or to increase the solid content while maintaining the same viscosity, ceramic particles of different sizes can be used [17].

For the curing behavior of a pure resin without a ceramic component, the Jacobs equation [18] can be used as a first approximation of the curing depth c_d. For ceramic slurries, this equation must be adapted, since the scattering between the binder system and ceramic particles results in a change in light propagation. Therefore, a curing in lateral direction is caused, being specified by the curing width c_w. Numerous models have been developed to understand the curing behavior of ceramic slurries. The models presented by Griffith [19,20] represent one of the first approaches to describe the cure depth c_d. Here, the difference of the refractive indices of binder and ceramic as well as the interparticle distance are named as important factors. Further experimental work builds on the Griffith's model, but continues to retain the refractive index difference and the interparticle distance as influencing variables [21,22]. In addition, the Jacobs equation can also be adapted to describe the curing width c_w [23].

1.3. Bayesian optimization

As previously described, ceramic slurries consist of a variety of constituents. When using classical Design of Experiments (DoE), a large number of trials is necessary to optimize the slurry by varying the mixture composition. This effect is known as the "curse of dimensionality", according to which the number of trials often increases exponentially as the number of parameters increases linearly, assuming that an acceptable result is still to be obtained [24]. Furthermore, special mixture experimental designs have to be employed, since varying the share of one component influences the share of the remaining constituents, e.g. simplex or simplex centroid plans.

Recently, Bayesian optimization, a specific artificial intelligence (AI) approach, could be used to improve an optimization task under variation of given parameters within a limited number of trials. In contrast to conventional DoE approaches, Bayesian optimization is an iterative global optimization algorithm which adaptively learns from generated data. In every step, an internal surrogate model - typically a Gaussian process regression model - is trained/updated to model the relationship between input parameters and optimization objective(s). An acquisition function is defined to quantify the usefulness of new data points by balancing the prediction and uncertainty of the surrogate model. The input parameter space is sampled to determine the maximum of the acquisition function to suggest experiments, which either reduce the uncertainty of the surrogate model or are likely to reveal a new global optimum of the objective function [25].]. Bayesian optimization is frequently used in materials acceleration platforms and self-driving labs to optimize materials composition as well as synthesis and processing conditions in automated experiments [26], e.g. to optimize chemical synthesis conditions [27] or materials composition to find stable and active catalysts [28]. Bayesian optimization is particularly suitable when the behavior of the objective function is mostly unknown, i.e. a black box, is expensive to evaluate and can only be determined by targeted experiments [29,30]. At the current state, such optimization tasks include the improvement of hyperparameters for AI applications [31,32] or automated experimentation [33–35].

1.4. Research target

Due to the VPP process chain including a layer wise build-up by light-induced curing, a debinding step for binder-burnout and a sintering step for compacting the component under volume shrinkage, several defects including pores, cracks, delamination and surface defects may arise, as specifically described e.g. in [36]. To reduce the risk of defects, to decrease the volume shrinkage and to enhance the dimensional accuracy during debinding and sintering, the ceramic content in VPP slurries should be increased [8]. Due to the complex interactions in the binder system and the light curing process, Bayesian optimization is used to optimize the slurry composition. The frequently used ceramic aluminum oxide (Al_2O_3) is used for the optimization approach to ensure a sufficient transferability of the results. The components of the binder were determined on the basis of a previous work, in which already acceptable viscosity values and solid contents could be established [37]. Thus, only the individual shares of the constituents of the mixture were varied by the Bayesian optimization, but not the substances itself. The optimization was carried out regarding a maximization of the solid content, a limitation of the viscosity to workable range and a minimization of the curing width relative to the curing depth to ensure a high printing resolution.

2. Materials and methods

2.1. Raw materials

To be able to investigate the influence of the particle size distribution, aluminum oxide with 0.05 μm, 0.5 μm and 3 μm median diameter (d_{50}) was used (Final Advanced Materials, Freiburg, Germany). For the binder system, three monomers with different functionality were used to investigate their influence on viscosity and curing behavior. Isobornyl acrylate (IBOA) was used as monofunctional monomer. Furthermore, 1,6-hexanediol diacrylate (HDDA) and trimethylolpropanethoxylate-triacrylate (TEMPTA) were used as di- and trifunctional monomers, respectively. Based on the 460 nm wave length of the curing unit of the VPP machine Lithoz 2M30 Science (Vienna, Austria) used, Camphorquinone (CQ) was chosen to be the photoinitiator together with 4-(dimethylamino)-benzonitrile as co-photoinitiator. As liquefying agent, 1-octanol was used. All stated substances were purchased by TCI Deutschland (Eschborn, Germany). Disperbyk (BYK-Chemie, Wesel, Germany) was used as a rheology additive. Table 1 provides an overview of the substances used and their main properties. In addition, the proportion of the respective substances in the initial mixture is given. Ceramic particles with a median diameter of 0.5 μm were used for the initial mixture.

Table 1
Properties of the substances used and their proportion in the initial mixture.

Name	Abbreviation	Density	Molar mass	Refractive index	Initial mixture	Initial mixture
Unit		g/cm^3	g/mol	-	vol.%	wt.%
Aluminum oxide	Al_2O_3	3.96	102.0	1.77	45.3	76.5
Isobornyl acrylate	IBOA	0.99	208.3	1.48	7.2	3.0
1,6-hexanediol diacrylate	HDDA	1.02	226.3	1.46	17.3	7.5
Trimethylolpropanethoxylate-triacrylate	TEMPTA	1.11	428.0	1.471	7.5	3.6
Camphorquinone	CQ	0,98	166.2	-	4.8	2.0
4-(dimethylamino)- benzonitrile	-	1,33	146.2	-	2.4	1.4
1-octanol	-	0.83	130.2	1.43	12.3	4.4
Disperbyk	-	1.16	-	-	3.2	1.6

2.2. Implementation of Bayesian optimization

Bayesian optimization uses a probabilistic surrogate model to determine an a posteriori probability distribution of the objective function using a data set consisting of parameters and measured values. The parameters are used to uniquely define the conditions under which a trial is performed. The measured values can include mean values as well as the corresponding measurement uncertainties. For the implementation, this work relied on the Ax software package (Meta Platforms, Menlo Park, USA) [38]. Ax provides a high-level application programming interface (API) to perform a multi-objective Bayesian optimization considering input and output constraints.

2.2.1. Parameters

The choice and number of parameters is crucial to be able to achieve optimization success. The number of parameters should not be too large in order not to unnecessarily increase the dimensionality of the search space and thus, the number of trials. However, the number of parameters should also not be too small in order to meet the complexity of the curing behavior and the relationship between solid content and viscosity. Therefore, the parameters should be selected in such a way that they are expected to have a significant influence on the target values mentioned.

Based on the literature reviewed, the particle size distribution has an influence on the viscosity [8,9,39,40]. Hence, the first three parameters w_{c1}, w_{c2} and w_{c3} were chosen to correspond to the mass fractions of the 0.05 μm, 0.5 μm and 3 μm aluminum oxide powder. In addition, the valid range of values for each ceramic powder was set between 0 and 90 wt.%. Setting the lower limit to 0 wt.% allows the option for the optimization to test a mono- or bimodal mixture. Furthermore, the total percentage of ceramic powder w_c (see formula 1) should be within a practical range.

$$w_c = \sum_{i=1}^{3} w_{ci} \tag{1}$$

While trials with a high ceramic content are desirable and thus permitted, trials with a too high ceramic content of $>$ 90 wt. % are excluded, as they can be expected to be unmixable. A lower limit is defined to avoid too low viscosities, which also impede the VPP process, and to reduce debinding problems based on a too low ceramic content. Therefore, the permitted range was set to be between 75wt. % and 90 wt. % as input constraint (see formula 2).

$$75\ \text{wt.\%} \leq w_c \leq 90\ \text{wt.\%} \tag{2}$$

For practical reasons, the shares are specified in wt.% in the experimental procedure, while the values are converted into vol.%, which is more meaningful for debinding and sintering.

As a fourth parameter q_{multi}, the share of multifunctional monomers (HDDA and TEMPTA) in comparison to the total mass of monomers (IBOA, HDDA and TEMPTA) was chosen (see formula 3), since it can be assumed that the monomer composition significantly influences the curing behavior by cross-linking [10].

$$q_{multi} = \frac{q_{HDDA} + q_{TEMPTA}}{q_{IBOA} + q_{HDDA} + q_{TEMPTA}} \tag{3}$$

In addition, a different composition of the monomer system also leads to a change in viscosity, since with increasing molar mass (see Table 1), the viscosity generally also increases [41]. The valid value range of q_{multi} is between 0 and 100 wt.% in order to be able to realize a monomer mixture consisting entirely of IBOA or HDDA and TEMPTA.

The four presented parameters provide information about the varied quantities. However, even if all four parameters are known, it is not possible to produce a mixture in a defined way, since there are more constituents in the slurry. Therefore, the initial mixture (see Table 1) is used to define some relative mixing ratios which are kept constant throughout the optimization. Thus, the overall share of monomers, initiator system, octanol and Disperbyk in the binder system are kept constant according to the initial mixture. In addition, the ratio of HDDA to TEMPTA is also defined. In combination with the four selected parameters, a unique ceramic slurry can be produced.

2.2.2. Objectives

As mentioned in the introduction, several objectives are to be improved by the optimization. Since it cannot be assumed that maximizing the solid content is accompanied by minimizing the viscosity, it is generally valid that there is no single, optimal solution in multi-objective optimization. Instead, a subset forms the pareto-optimal solutions, whose individual objective values can no longer be improved without not worsening at least one other objective value. Therefore, the (parallel) noisy expected hypervolume improvement (qNEHVI) algorithm [42] as implemented in Ax was used to increase the noisy Pareto front as best as possible.

The first objective is a maximization of the total ceramic content w_c. Although w_c could be determined directly by summation of w_{c1} to w_{c3}, the relationship between the parameters and the objective was considered as a black box for simpler implementation. Another reason for the implementation as a black box is the required possibility to assign a minimum solid content as a penalty to mixtures that cannot be processed (e.g. as a result of a too high ceramic content).

The second objective takes the viscosity η into account. In scientific literature, different viscosity values, which were determined at different shear rates, were considered as permissible [8]. Therefore, it is beneficial to optimize the viscosity not only to a specific value, but to consider a certain range of values as optimal. Furthermore, in addition to this optimum range, viscosity values can also be considered as still workable,

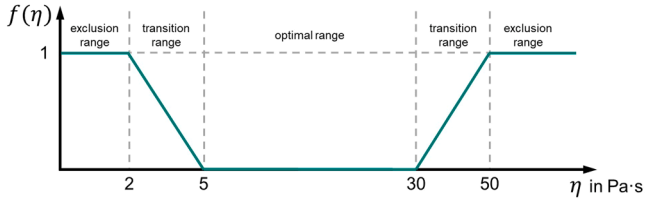

Fig. 1. Schematic depiction of the viscosity function

but no longer ideal. In the context of this paper, a section-wise defined viscosity function $f(\eta)$ is introduced as an objective that maps these ranges. The viscosity function is zero for the optimum range and increases linearly to one in the still valid transition range (see Fig. 1). The optimum range and the transition range are defined by four viscosity values ($\eta_{min,1}$= 2 Pa·s, $\eta_{min,0}$ = 5 Pa·s, $\eta_{max,0}$ = 30 Pa·s, $\eta_{max,1}$ = 50 Pa·s) on the basis of empirical knowledge and pertinent literature. The aim of the optimization is then to minimize $f(\eta)$.

The experimental measurement of the viscosity value η is described later in Section 2.3. In addition to the viscosity function, output constraints for the viscosity have been implemented to require the viscosity to remain within the smallest and largest viscosity values defining the viscosity function. It should be noted, however, that there is no guarantee that the output constraints will be met. Instead, Bayesian optimization models the probability that the conditions will be fulfilled.

The final third objective considers the widening of the cured area. To achieve a high dimensional accuracy, a large cure depth c_d and a small cure width c_w are striven. Therefore, the widening angle α, consisting of the ratio of c_w and c_d (see formula 4), is introduced as the objective to be minimized. The determination of c_w and c_d is also described in more detail in Section 2.3.

$$\alpha = \arctan\left(\frac{c_w}{c_d}\right) \tag{4}$$

2.3. Experimental procedure

First, the general experimental procedure is described, followed by a more detailed description of the second process step, being the major experimental setup. The general experimental workflow is as follows:

1. N = 4 randomized sets of parameters for a mixture are chosen as a starting point.
2. The sample, i.e. the slurry, is prepared by mixing the individual constituents. The objective values are determined by rheology and curing measurements. The corresponding values are available in each instance as mean values and standard deviations, which indicate the measurement uncertainty. The data tuple determined in this way from parameters and measured values expands the available data set.
3. Bayesian optimization determines a new parameter set for the evaluation based on the additional data.
4. The process, i.e. steps 2 and 3, is repeated iteratively.

A total of 30 g of ceramic slurry was prepared for each sample. A common laboratory scale (Kern PCB 2500, Balingen, Germany) was used for weighing the constituents. Since the mixture compositions suggested by the Bayesian optimization could not be exactly fulfilled due to manual weighing, the actual values, being as close as possible to the suggest values, were used as further input for the Bayesian optimization. The measurement uncertainty of the scale was determined, in addition to the official calibration certificate issued by Deutsche Akkreditierungsstelle, once before the experiments were carried out, by measuring ten times a reference weight and calculating the corresponding standard deviation. The measurement uncertainty was then assumed to be constant for all further weighing operations.

Ceramic balls (20 pieces, 90 % Al_2O_3, 5.0 - 7.0 mm diameter) were added to the sample container to achieve improved mechanical mixing. The mixing took place in a high-speed centrifugal mixer (Thinky ARE-250, C3 Prozess- und Analysetechnik, Haar, Germany). The same mixing procedure was followed for each sample. Following the specifications of the mixer manufacturer, first the liquids and then the powders (aluminum oxide, initiator system) were added to the sample container. The mechanical mixing consisted of two steps, which were repeated alternately: A mixing phase with a duration of 60 s at 2,000 rpm and a rest phase of 120 s, in which the container was not rotated. In total, three mixing phases and two rest phases took place. In addition, the temperature was controlled by a sensor attached to the mixing container (Thinky Multi-Sensor, C3 Prozess- und Analysetechnik, Haar, Germany) to avoid thermal curing or other slurry modifications as a result of too high temperatures caused by an unsuitable mixing process.

The slurries' viscosity was determined by rotational measurements using a plate-plate geometry with 20 mm diameter on a rheometer (Haake Mars 40, ThermoFisher Scientific, Karlsruhe, Germany). The shear rate depends on the layer thickness and the recoating speed. Since the shear rates vary depending on the used VPP machine and the selected process parameters, especially in rotationally coating systems, like the majority of the ceramic VPP systems provided by Lithoz (Vienna, Austria), the viscosity is measured in a shear rate interval to increase the validity of the optimization. Based on typical VPP machines, the evaluation interval was set to a shear rate of 200 to 1,000 1/s, while the measurement interval was between 0 and 1,200 1/s to avoid possible measurement errors at very low or high shear rates. To exclude outliers for the viscosity value, the maximum value remaining after disregarding the upper five percent of the viscosity values within the evaluation interval was set as the viscosity η. To guarantee the numerical stability of the Bayesian optimization, a standard deviation of 1 % was also assumed.

The determination of the viscosity value is illustrated by Fig. 2, which shows exemplarily the measurement results of the 38th trial. In addition to the measurement interval and the gray-shaded evaluation interval, the different viscosity values can be seen as described above.

For determining the widening angle, samples of cured slurry were prepared on which c_d and c_w could be determined. For the exposure, a 2M30 Science VPP system from Lithoz employing the bottom-up principle, was used. A transparent foil (thickness 30 μm) was placed on the transparent vat of the system, onto which the liquid ceramic slurry of the respective trial was applied. In order to determine the cure depth, an exposure pattern was created with five circles of diameter 5 mm. For the curing width, five squares with an edge length of 4 mm were arranged analogously. In addition, the squares were arranged specifically in multiples of the resolution of the projector by the so-called bounding box principle. The distance between all geometries was larger 8 mm to avoid mutual interactions due to light scattering. Additional measurements were also taken in advance to ensure that the exposure by the projector was uniform in intensity over the entire area. Exposure for all samples was at an intensity of 40 mW/cm^2 with an exposure time of 4.3 s, resulting in a total energy of 175 mJ/cm^2. After exposure, the foil with the slurry was removed and cleaned by wiping the uncured slurry with the aid of isopropanol (VWR International, Darmstadt, Germany). By measuring the thickness of the circular objects using a micrometer (Micromahr, Mahr, Göttingen, Germany), the mean and standard deviation of c_d was determined. The thickness of the foil was measured in advance and subtracted from the measured value. Images of the square

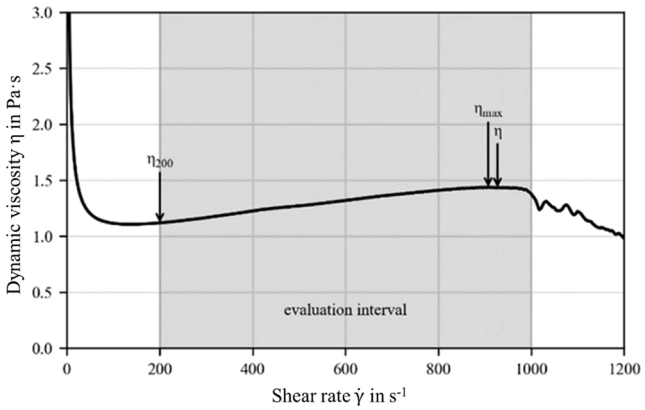

Fig. 2. Viscosity profile of the 38th trial

objects were taken with the aid of a light microscope (Axio Imager M1m, Carl Zeiss Microscopy, Germany) and analyzed by the open-source software ImageJ [43]. The cure width c_w was then taken to be the additional edge length that the target area, assumed to be a square, is greater than the actual area. With the mean values and standard deviations of c_d and c_w now known, the mean value and standard deviation of the widening angle could be determined using the law of error propagation.

A total of 44 tests were performed using the procedure just described. The first four trials were performed with random parameters to ensure the numerical stability of Bayesian optimization, while all other trials were implemented iteratively by applying the qNEHVI algorithm. Each sample was measured immediately after mixture preparation, so each sample run took about 2 to 3 h. Some of the samples were not mixable, e.g. due to a too high ceramic content, so that the subsequent measurements could not be performed. Worst-case values were then taken for these samples, i.e. $\alpha = 90°$ and $\eta = 530$ Pa·s, the highest viscosity value of the first mixtures.

3. Results

3.1. Solid content and viscosity

A first aspect of interest is the relationship between the ceramic content and the viscosity or the viscosity function, respectively. Fig. 3 shows the measured viscosity values in dependency of the total ceramic content, suggested by Bayesian optimization.

Colored measurement points, whose number corresponds to the trial in the optimization, form the Pareto front and therefore, the set of optimal solutions. The error bars correspond to the $\pm 2\sigma$-confidence interval of the measured values and are only visible for the ceramic content in the figure. The additional gray measuring points visualize trials that did not lead to Pareto-optimal results. In the background, the ranges of the viscosity function (transition range and invalid range) are also illustrated by different gray shades; the optimal range remains white. The figure illustrates that over the entire permissible range of values of the ceramic fraction (75 to 90 wt.%) samples were examined by the optimization. The sample values follow the generally expected course: as the ceramic content increases, so does the viscosity. Furthermore, it can be seen that Bayesian optimization succeeded in achieving improved viscosities for samples with approximately the same ceramic content in the course of optimization. This is an indication that the choice of parameters has a significant influence on the viscosity. It is noticeable that the resulting Pareto front can be described as increasing exponentially, which is similar to well-known model equations, such as the Krieger-Dougherty equation [44].

Table 2
Properties of the best mixture composition within the optimum range of the viscosity function.

Name	Value
w_c	65.24 vol.%, 88.41 wt.%
η (Used for optimization)	12.988 Pa*s
η_{max} (Maximum value in measuring range)	14.132 Pa*s
η_{200} (Viscosity at a shear rate of 200 1/s)	8.478 Pa*s
q_{multi}	10.58%
w_{c1} (Relative to w_c)	18.00%
w_{c2} (Relative to w_c)	34.79%
w_{c3} (Relative to w_c)	47.21%

The range of samples that lie in the optimum range of the viscosity function is between about 84 and 88.4 wt.%, corresponding to 62 to 65 vol.%. All other samples with a lower ceramic content, were too thin to reach the minimum required viscosity of 2 Pa·s, as can be seen from Fig. 3, e.g. mixtures 11 and 13. Similar effects were described for example in [45]. Therefore, they are in the invalid range of the viscosity function, besides the high risk of defects caused by thermal postprocessing.

The sample with a maximum ceramic content still being within the optimum range of the viscosity function, was produced in the 40th trial. Table 2 shows the obtained ceramic content w_c in mass and volume percent as well as the viscosity η (used for optimization), the maximum viscosity η_{max} over the measuring range and the viscosity η_{200} at a shear rate of 200 1/s. Furthermore, the parameters for the mixture composition are given.

The successfully prepared aluminum oxide suspension has a ceramic content of 65.24 vol.% at a maximum viscosity of 14.32 Pa·s within the measurement interval. At the present time, this suspension has the highest aluminum oxide content at comparable viscosities known to the authors. The prepared mixture exceeds, for example, the values presented by Zhang (60 vol.%, 15.4 Pa·s at 200 1/s, [46]) or Hu (60 vol.%, 3.11 Pa·s at unknown shear rate, [47]) for ceramic suspensions with a high solid content. In relation to the initial mixture, the volume content could thus be increased relatively by 44%.

Furthermore, it is noticeable that the three Pareto-optimal mixtures with the largest ceramic content have comparable particle size distributions. As the particle diameter increases, so does the relative proportion of ceramic content: $w_{c1} < w_{c2} < w_{c3}$. In particular, the 40th trial approximately follows the composition theory of an ideal trimodal suspension predicted by Farris [17], which provides for a 66 vol.% mixture 22, 32, and 46 relative vol.% of small, medium and large particles, respectively.

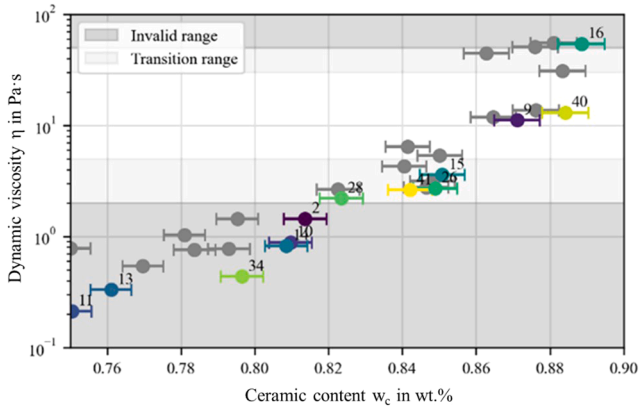

Fig. 3. Measured dynamic viscosities in dependency of the ceramic content for all mixtures suggested by Bayesian optimization

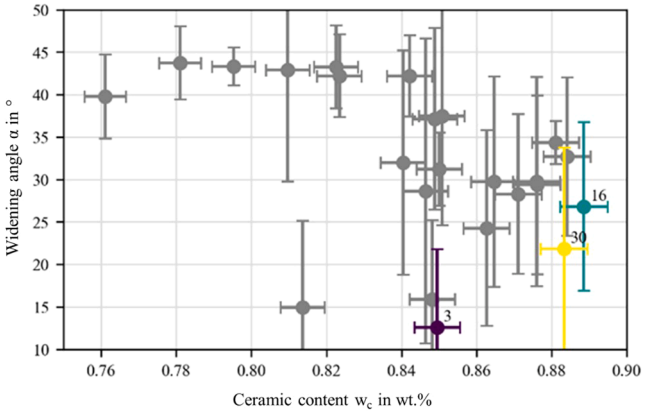

Fig. 4. Measured widening angle in dependency of the ceramic content for all mixtures suggested by Bayesian optimization

3.2. Cure widening

The results regarding the widening angle are shown in Fig. 4. The widening angles were plotted against the ceramic content. Furthermore, error bars describe the $\pm 2\sigma$-confidence interval of the measured values. The set of pareto-optimal solutions is plotted in color, while all other measured values are plotted in gray.

It is noticeable that the majority of the widening angles show a strong variance. Therefore, it is only possible to a limited extent to attribute a minimization of the widening angle with similar total ceramic content to a change in the parameters. A possible Pareto front is only covered by samples 3, 16 and 30. In view of the total number of trials, it is not reasonable to assume a recognizable dependence between ceramic content and widening angle. Instead, it is more obvious to assume no correlation between the ceramic content and the widening angle. This assumption is also supported by the fact that no substance was used in the present mixture compositions strongly modifying the difference in refractive indices between the ceramic and the binder. However, the validity of the claim is weakened by the strong variation of the individual samples. The large variation in the widening angle is due to the large variation in the measurement of the curing width. While conducting the experiments, the cleanup of the cured square objects, especially in the edge contact between the cured and liquid slurry, proved to be somehow imprecise. The examined objects showed a transition area from clearly cured to clearly liquid slurry that can be attributed to light scattering. The extent of this transition area was different for each sample and, from experience, dependent on the viscosity of the ceramic slurry.

3.3. Comparison to conventional design of experiments (DoE) methods

When considering the results obtained by Bayesian optimization, the additional question arises whether conventional DoE methods can achieve similar optimal results within the same limited number of trials. Since performing real experiments again to assess several conventional DoE methods would be inefficient, a theoretical comparison between Bayesian optimization and selected other DoE methods was performed. The data basis for this is the data set of parameters and associated measured values already obtained by Bayesian optimization. Since the values of the widening angle are subject to strong noise, the comparison was limited to the relationship between ceramic content and viscosity.

For the comparison, two different DoE strategies were investigated: (quasi)random methods (here: random search, Latin hypercube [48] and Sobol sampling [49]) and deterministic methods (simplex and simplex centroid method). In random search, the individual parameters were determined independently for each trial according to a uniform distribution. The random parameter generation was repeated until the input boundary conditions were met. For Latin hypercube sampling (LHS), five parameters were used. In addition to the four parameters used in Bayesian optimization, a fifth parameter is necessary in this method to represent the total ceramic content (between 75 and 90 wt.%). In the LHS, each parameter is divided into n sections, where n corresponds to the number of trials. Subsequently, the parameters are randomly selected from these sections. Once a set of a parameter has been used, it is no longer available for further trials. This results in a uniform, quasi-random coverage of the search space. The goal of the Sobol method is, analogously to the LHS method, to generate a quasi-random distribution that has a more homogeneous coverage than a purely random distribution. Because of the formula underlying the procedure, the distribution is only homogeneous if $n = 2^m$ with m being a natural number. However, the Sobol method can also be used if this condition is not met.

For the deterministic DoE methods, the simplex-33 grid, simplex-32 grid, simplex-centroid grid and extended simplex-centroid grid were considered. The commonality of these methods is their attempt to uniformly cover the search space for a mixture composition. Thus, for ceramic slurry optimization, the parameters w_{c1}, w_{c2}, and w_{c3} can be specified relatively to the total ceramic content. In addition, a full factorial experimental design was applied for the total ceramic content (75, 80, 85, and 90 wt.%) and q_{multi} ratio (0, 50, 100 wt.-%), resulting in, for example, $7 \cdot 4 \cdot 3 = 84$ trials for the simplex centroid method with seven grid points. To minimize the random influence of the trials' order, the quasi-random procedures were repeated 10,000 times with new parameters. For the simplex procedures, the arrangement of the procedures was randomly changed 10,000 times accordingly. This procedure made it possible to determine for each trial number the average maximum ceramic content achieved up to that trial. The ceramic content and viscosity were determined by interpolation from the data set obtained by Bayesian optimization. If a parameter set of the comparison methods was within the convex hull of the data set, linear interpolation was used. If a parameter set was outside the convex hull, the nearest data point was assigned to the parameters.

Fig. 5 shows the results of the comparison. For both, Bayesian optimization and the other DoE methods, the maximum ceramic content achieved up to the respective trial are shown, which still fulfill the outer limits of the viscosity function.

The Bayesian optimization converges towards 88.41 wt.%, which is reached from the 40th trial on. In addition, it was already possible in the fifth trial to produce a slurry that is within the defined viscosity limits. From the compared methods, the Sobol method leads to the best result, while the simplex centroid method with the connected full factorial experimental design converges the worst. It is noticeable that on average, none of the comparison methods is able to converge as fast and as strongly as the Bayesian optimization. However, it must be mentioned that due to the linear interpolation it is not possible for the comparison methods to find a better result than the result determined by Bayesian optimization. Indeed, since the best result determined by Bayesian optimization is very large in relation to the results obtained in the scientific literature [46] and additionally follows the theory of Farris [17], it can be considered that this result is at least a very good local optimum. In conclusion, it can be stated that Bayesian optimization based on the theoretical comparison is clearly superior to the other DoE methods.

4. Discussion

One of the objectives of the work was to produce a slurry with maximum ceramic content while maintaining defined viscosity limits. Bayesian optimization has made it possible to obtain a Pareto front over the entire width of the desired ceramic content (75 to 90 wt.%). The exponential curve is similar to well-known model equations, such as the Krieger-Dougherty equation for describing the dependence of solid content and viscosity of a suspension. It can therefore be concluded that the Krieger-Dougherty equation can also be applied to multimodal

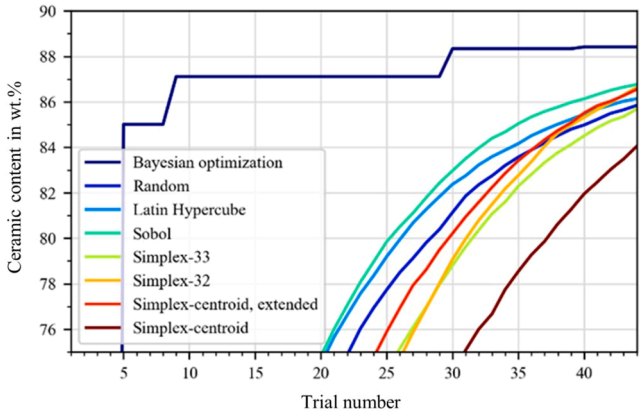

Fig. 5. Comparison of the maximum ceramic content achieved within the permissible viscosity limits for different DoE methods

ceramic mixtures. In addition to the exponential course of the Pareto front, it was also possible to produce mixtures with very high ceramic content at comparatively moderate and workable viscosities. The aluminum oxide slurry prepared in the 40th trial represents the suspension with the highest ceramic content known to the authors. Since the relative size distribution of the ceramic particles additionally follows the Farris theory, which has also been enhanced by further publications [50–52], it can be assumed that the developed solution is close to the global optimum. Bayesian optimization is therefore suitable for achieving outstanding results within a limited number of experiments, which probably cannot be achieved by conventional experimental design methods, as the theoretical comparison in Section 3.1.3 suggests.

Regarding the minimization of the widening during the curing process, no correlation between the choice of parameters and the expansion could be found. In retrospect, a different experimental procedure for determining the cure width with a smaller variance would have increased the validity of the Bayesian optimization with respect to the widening angle. In addition, the uncertain measurement results of the cure width also worsen the optimization capability of Bayesian optimization with respect to the other objectives. However, Bayesian optimization nevertheless succeeded in producing a ceramic slurry with a very high solid content within the viscosity limits, which underlines the ability of Bayesian optimization to perform successful optimization even under partially highly noisy measurement results. Due to the parameters known from literature [19,20] (esp. the refractive indices of ceramic and binder), which influence the scattering behavior of the ceramic suspension and were not adjusted in this work, the measurement results can nevertheless be interpreted to the effect that there is no clear correlation between the ceramic fraction and the widening angle.

A challenge that accompanies a high ceramic content is the stability of the slurries. Especially slurries with high ceramic content tend to separate and the ceramic particles tend to build agglomerates and therefore, to sediment [53]. The slurries prepared in this work fulfilling the required viscosity limits were also sufficiently stable for printing several layers. By the continuous agitation during the layer application, the slurry is regularly mixed within the VPP machine. However, the slurries showed the first signs of sedimentation after standing for a longer time without any movement. Therefore, the composition needs to be further optimized regarding an industrial application of the slurries, especially by adding optimized dispersion agents that enhance the stability of the particles within the slurry [8,9].

5. Conclusion and outlook

In the present work, an aluminum oxide suspension was optimized by the iterative interplay between Bayesian optimization and experimental mixture preparation and evaluation. The results obtained represent a new peak in terms of total ceramic content. The work was therefore able to show that Bayesian optimization as a learning and thus adaptive method has considerable advantages over conventional DoE methods. It underlines the aspiration of Bayesian optimization to be an advantageous method for the optimization of mixture compositions, as it is already the case for autonomous experimentation or the optimization of hyperparameters.

No improvement could be obtained for minimizing the lateral expansion during curing. Besides an improvement of the determination of the curing width, future work may additionally try to adjust the refractive index of the binder in order to be able to investigate its influence on the expansion behavior.

Furthermore, another research aspect is the optimization of the entire VPP process chain including debinding and sintering. Up to now, it remains unclear, up to what extent an optimization of the ceramic slurry leads to an improvement of the properties of the final part and how the dependencies between the individual process steps can be optimized. Therefore, an optimized algorithm employing batch processes for debinding and sintering has to be employed.

CRediT authorship contribution statement

Johannes Schubert: Writing – review & editing, Validation, Project administration, Methodology, Investigation, Formal analysis, Conceptualization. **Pascal Friederich:** Writing – review & editing, Validation, Supervision, Software, Resources, Funding acquisition, Formal analysis, Conceptualization. **Benedikt Burchard:** Writing – original draft, Visualization, Validation, Software, Methodology, Investigation, Formal analysis, Data curation. **Frederik Zanger:** Writing – review & editing, Validation, Supervision, Resources, Funding acquisition, Conceptualization.

Declaration of competing interest

The authors declare that they have no known competing financial interests or personal relationships that could have appeared to influence the work reported in this paper.

Supplementary materials

Supplementary material associated with this article can be found, in the online version, at doi:10.1016/j.oceram.2024.100705.

References

[1] M. Schwentenwein, J. Homa, Additive manufacturing of dense alumina ceramics, Int. J. Appl. Ceram. Technol. 12 (2015) 1–7, https://doi.org/10.1111/ijac.12319.
[2] X. Tian, D. Li, Z. Chen, W. Zhou, Study on the fabrication accuracy of ceramic parts by direct stereolithography, Virt. Phys. Prototyp. 7 (2012) 195–202, https://doi.org/10.1080/17452759.2012.718492.
[3] A. Zocca, P. Colombo, C.M. Gomes, J. Günster, Additive manufacturing of ceramics: issues, potentialities, and opportunities, J. Am. Ceram. Soc. 98 (2015) 1983–2001, https://doi.org/10.1111/jace.13700.
[4] U. Scheithauer, E. Schwarzer, T. Moritz, A. Michaelis, Additive manufacturing of ceramic heat exchanger: opportunities and limits of the lithography-based ceramic manufacturing (LCM), J. Mater. Eng. Perform. 27 (2018) 14–20, https://doi.org/10.1007/s11665-017-2843-z.
[5] N. Travitzky, A. Bonet, B. Dermeik, T. Fey, I. Filbert-Demut, L. Schlier, T. Schlordt, P. Greil, Additive manufacturing of ceramic-based materials, Adv. Eng. Mater. 16 (2014) 729–754, https://doi.org/10.1002/adem.201400097.
[6] E. Schwarzer-Fischer, J. Abel, J. Sieder-Katzmann, M. Propst, C. Bach, U. Scheithauer, A. Michaelis, Study on CerAMfacturing of novel alumina aerospike nozzles by lithography-based ceramic vat photopolymerization (CerAM VPP), Mater. (Basel) (2022) 15, https://doi.org/10.3390/ma15093279.
[7] J. Homa, M. Schwentenwein, A Novel Additive Manufacturing Technology for High-Performance Ceramics, Advanced Processing and Manufacturing Technologies for Nanostructured and Multifunctional Materials: A Collection of Papers Presented at the 38th International Conference on Advanced Ceramics and Composites January 27–31 (2014) 33–40. https://doi.org/10.1002/9781119040354.ch4.
[8] S. Zakeri, M. Vippola, E. Levänen, A comprehensive review of the photopolymerization of ceramic resins used in stereolithography, Addit. Manufact. 35 (2020) 101177, https://doi.org/10.1016/j.addma.2020.101177.
[9] I.L. de Camargo, M.M. Morais, C.A. Fortulan, M.C. Branciforti, A review on the rheological behavior and formulations of ceramic suspensions for vat photopolymerization, Ceram. Int. 47 (2021) 11906–11921, https://doi.org/10.1016/j.ceramint.2021.01.031.
[10] X. Xu, S. Zhou, J. Wu, Y. Liu, Y. Wang, Z. Chen, Relationship between the adhesion properties of UV-curable alumina suspensions and the functionalities and structures of UV-curable acrylate monomers for DLP-based ceramic stereolithography, Ceram. Int. 47 (2021) 32699–32709, https://doi.org/10.1016/j.ceramint.2021.08.166.
[11] J. Jakubiak, X. Allonas, J.P. Fouassier, A. Sionkowska, E. Andrzejewska, L. Linden, J.F. Rabek, Camphorquinone–amines photoinitating systems for the initiation of free radical polymerization, Polymer 44 (2003) 5219–5226, https://doi.org/10.1016/S0032-3861(03)00568-8.
[12] I.V. Khudyakov, Fast photopolymerization of acrylate coatings: achievements and problems, Progr. Organ. Coat. 121 (2018) 151–159, https://doi.org/10.1016/j.porgcoat.2018.04.030.
[13] A. Bertsch, S. Jiguet, P. Renaud, Microfabrication of ceramic components by microstereolithography, J. Micromech. Microeng. 14 (2004) 197–203, https://doi.org/10.1088/0960-1317/14/2/005.
[14] W. Zimbeck, R. Rice, Stereolithography of ceramics and metals, IS&T's 50th Annu. Confer. (1997) 649–655.
[15] G.A. Brady, T.-M. Chu, J.W. Halloran, Curing Behavior of Ceramic Resin for Stereolithography, in: 1996 International Solid Freeform Fabrication Symposium, 1996.

[16] C.-J. Bae, A. Ramachandran, K. Chung, S. Park, Ceramic stereolithography: additive manufacturing for 3D complex ceramic structures, J. Korea. Ceram. Soc 54 (2017) 470–477, https://doi.org/10.4191/kcers.2017.54.6.12.
[17] R.J. Farris, Prediction of the viscosity of multimodal suspensions from unimodal viscosity data, Transact. Soc. Rheol. 12 (1968) 281–301, https://doi.org/10.1122/1.549109.
[18] P.F. Jacobs, Fundamentals of Stereolithography, 1992 international solid freeform fabrication symposium (1992).
[19] M.L. Griffith, J.W. Halloran, Freeform fabrication of ceramics via stereolithography, J. Am. Ceram. Soc. 79 (1996) 2601–2608.
[20] M.L. Griffith, J.W. Halloran, Scattering of ultraviolet radiation in turbid suspensions, J. Appl. Phys. 81 (1997) 2538–2546, https://doi.org/10.1063/1.364311.
[21] V. Tomeckova, J.W. Halloran, Cure depth for photopolymerization of ceramic suspensions, J. Eur. Ceram. Soc. 30 (2010) 3023–3033, https://doi.org/10.1016/j.jeurceramsoc.2010.06.004.
[22] J.H. Jang, S. Wang, S.M. Pilgrim, W.A. Schulze, Preparation and characterization of barium titanate suspensions for stereolithography, J. Am. Ceram. Soc. 83 (2000) 1804–1806, https://doi.org/10.1111/j.1151-2916.2000.tb01467.x.
[23] S.P. Gentry, J.W. Halloran, Depth and width of cured lines in photopolymerizable ceramic suspensions, J. Eur. Ceram. Soc. 33 (2013) 1981–1988, https://doi.org/10.1016/j.jeurceramsoc.2013.02.033.
[24] R. Bellman, Dynamic Programming, Sixth. printing, Univ. Pr, Princeton, N.J., 1972.
[25] J. Mockus, Bayesian Approach to Global Optimization, Kluwer Academic Publishers, Dordrecht, 1989.
[26] P.M. Maffettone, P. Friederich, S.G. Baird, B. Blaiszik, K.A. Brown, S.I. Campbell, O.A. Cohen, R.L. Davis, I.T. Foster, N. Haghmoradi, M. Hereld, H. Joress, N. Jung, H.-K. Kwon, G. Pizzuto, J. Rintamaki, C. Steinmann, L. Torresi, S. Sun, What is missing in autonomous discovery: open challenges for the community, Digit. Discov. 2 (2023) 1644–1659, https://doi.org/10.1039/D3DD00143A.
[27] B.J. Shields, J. Stevens, J. Li, M. Parasram, F. Damani, J.I.M. Alvarado, J.M. Janey, R.P. Adams, A.G. Doyle, Bayesian reaction optimization as a tool for chemical synthesis, Nature 590 (2021) 89–96, https://doi.org/10.1038/s41586-021-03213-y.
[28] K.J. Jenewein, L. Torresi, N. Haghmoradi, A. Kormányos, P. Friederich, S. Cherevko, Navigating the unknown with AI: multiobjective Bayesian optimization of non-noble acidic OER catalysts, J. Mater. Chem. A 12 (2024) 3072–3083, https://doi.org/10.1039/D3TA06651G.
[29] D.R. Jones, M. Schonlau, W.J. Welch, Efficient Global Optimization of Expensive Black-Box Functions, J. Glob. Optimiz. 13 (1998) 455–492.
[30] E. Brochu, V.M. Cora, N.d. Freitas, A Tutorial on Bayesian Optimization of Expensive Cost Functions, with Application to Active User Modeling and Hierarchical Reinforcement Learning (2010).
[31] J. Snoek, H. Larochelle, R.P. Adams, practical Bayesian optimization of machine learning algorithms, Adv. Neur. Inform. Process. Syst. 25 (2012).
[32] A. Klein, S. Falkner, S. Bartels, P. Hennig, F. Hutter, Fast Bayesian Optimization of Machine Learning Hyperparameters on Large Datasets, in: Proceedings of the 20th International Conference on Artificial Intelligence and Statistics (AISTATS), 2017.
[33] A.E. Gongora, B. Xu, W. Perry, C. Okoye, P. Riley, K.G. Reyes, E.F. Morgan, K. A. Brown, A Bayesian experimental autonomous researcher for mechanical design, Sci. Adv. 6 (2020) eaaz1708, https://doi.org/10.1126/sciadv.aaz1708.
[34] S. Langner, F. Häse, J.D. Perea, T. Stubhan, J. Hauch, L.M. Roch, T. Heumueller, A. Aspuru-Guzik, C.J. Brabec, Beyond ternary OPV: high-throughput experimentation and self-driving laboratories optimize multicomponent systems, Adv. Mater. 32 (2020) e1907801, https://doi.org/10.1002/adma.201907801.
[35] B.P. MacLeod, F.G.L. Parlane, T.D. Morrissey, F. Häse, L.M. Roch, K.E. Dettelbach, R. Moreira, L.P.E. Yunker, M.B. Rooney, J.R. Deeth, V. Lai, G.J. Ng, H. Situ, R. H. Zhang, M.S. Elliott, T.H. Haley, D.J. Dvorak, A. Aspuru-Guzik, J.E. Hein, C. P. Berlinguette, Self-driving laboratory for accelerated discovery of thin-film materials, Sci. Adv. 6 (2020) eaaz8867, https://doi.org/10.1126/sciadv.aaz8867.
[36] K. Zhang, Q. Meng, Z. Qu, R. He, A review of defects in vat photopolymerization additive-manufactured ceramics: Characterization, control, and challenges, J. Eur. Ceram. Soc. 44 (2024) 1361–1384, https://doi.org/10.1016/j.jeurceramsoc.2023.10.067.
[37] J. Schubert, C.-L. Lehmann, F. Zanger, Versatile binder system as enabler for multi-material additive manufacturing of ceramics by vat photopolymerization, Ceram. Int. (2024), https://doi.org/10.1016/j.ceramint.2024.10.006.
[38] M. Balandat, B. Karrer, D.R. Jiang, S. Daulton, B. Letham, A.G. Wilson, E. Bakshy, BoTorch: A Framework for Efficient Monte-Carlo Bayesian Optimization, Adv. Neur. Inform. Process. Syst. 33 (2020).
[39] X. Li, H. Zhong, J. Zhang, Y. Duan, J. Li, D. Jiang, Fabrication of zirconia all-ceramic crown via DLP-based stereolithography, Int. J. Appl. Ceram. Technol. 17 (2020) 844–853, https://doi.org/10.1111/ijac.13441.
[40] X.-B. Li, H. Zhong, J.-X. Zhang, Y.-S. Duan, D.-L. Jiang, Powder characteristics on the rheological performance of resin-based zirconia suspension for stereolithography, J. Inorgan. Mater. 35 (2020) 231–235, https://doi.org/10.15541/jim20190091.
[41] B. Oezkan, F. Sameni, S. Karmel, D.S. Engstrøm, E. Sabet, A systematic study of vat-polymerization binders with potential use in the ceramic suspension 3D printing, Addit. Manufact. 47 (2021) 102225, https://doi.org/10.1016/j.addma.2021.102225.
[42] S. Daulton, M. Balandat, E. Bakshy, Parallel bayesian optimization of multiple noisy objectives with expected hypervolume improvement, Adv. Neur. Inform. Process. Syst. 34 (2021) 2187–2200.
[43] C.A. Schneider, W.S. Rasband, K.W. Eliceiri, NIH Image to ImageJ: 25 years of image analysis, Nat. Method. 9 (2012) 671–675, https://doi.org/10.1038/nmeth.2089.
[44] I.M. Krieger, T.J. Dougherty, A mechanism for non-newtonian flow in suspensions of rigid spheres, Transact. Soc. Rheol. 3 (1959) 137–152, https://doi.org/10.1122/1.548848.
[45] E. Schwarzer-Fischer, E. Zschippang, W. Kunz, C. Koplin, Y.M. Löw, U. Scheithauer, A. Michaelis, CerAMfacturing of silicon nitride by using lithography-based ceramic vat photopolymerization (CerAM VPP), J. Eur. Ceram. Soc. 43 (2023) 321–331, https://doi.org/10.1016/j.jeurceramsoc.2022.10.011.
[46] K. Zhang, C. Xie, G. Wang, R. He, G. Ding, M. Wang, D. Dai, D. Fang, High solid loading, low viscosity photosensitive Al2O3 slurry for stereolithography based additive manufacturing, Ceram. Int. 45 (2019) 203–208, https://doi.org/10.1016/j.ceramint.2018.09.152.
[47] K. Hu, Y. Wei, Z. Lu, L. Wan, P. Li, Design of a shaping system for stereolithography with high solid loading ceramic suspensions, 3D Print. Addit. Manufact. 5 (2018) 311–318, https://doi.org/10.1089/3dp.2017.0065.
[48] M.D. McKay, R.J. Beckman, W.J. Conover, A comparison of three methods for selecting values of input variables in the analysis of output from a computer code, Technometrics 21 (1979) 239, https://doi.org/10.2307/1268522.
[49] I.M. Sobol', On the distribution of points in a cube and the approximate evaluation of integrals, Zhurnal Vychislitel'noi Matematiki i Matematicheskoi Fiziki 7 (1967) 784–802.
[50] A.A. Zaman, B.M. Moudgil, Rheology of bidisperse aqueous silica suspensions: A new scaling method for the bidisperse viscosity, J. Rheol. 42 (1998) 21–39, https://doi.org/10.1122/1.550935.
[51] R. Greenwood, P.F. Luckham, T. Gregory, Minimising the viscosity of concentrated dispersions by using bimodal particle size distributions, Colloid. Surf. A: Physicochem. Eng. Aspect. 144 (1998) 139–147, https://doi.org/10.1016/S0927-7757(98)00409-9.
[52] P.M. Mwasame, N.J. Wagner, A.N. Beris, Modeling the effects of polydispersity on the viscosity of noncolloidal hard sphere suspensions, J. Rheol. 60 (2016) 225–240, https://doi.org/10.1122/1.4938048.
[53] C.-J. Bae, J.W. Halloran, Concentrated suspension-based additive manufacturing – viscosity, packing density, and segregation, J. Eur. Ceram. Soc. 39 (2019) 4299–4306, https://doi.org/10.1016/j.jeurceramsoc.2019.05.034.